Journal of Catalysis 265 (2009) 35–42

Contents lists available at ScienceDirect

Journal of Catalysis

journal homepage: www.elsevier.com/locate/jcat

Theoretical elucidation of the selectivity changes for the hydrogenation of unsaturated aldehydes on Pt(1 1 1)

Slimane Laref, Françoise Delbecq, David Loffreda *

Université de Lyon, Institut de Chimie de Lyon, Laboratoire de Chimie, Ecole Normale Supérieure de Lyon, CNRS, 46 Allée d'Italie, F-69364 Lyon Cedex 07, France

ARTICLE INFO

Article history:
Received 3 February 2009
Revised 19 March 2009
Accepted 11 April 2009
Available online 28 May 2009

PACS:
68.10.Jy
82.65.Jv

Keywords:
Brönsted–Evans–Polanyi relation
Chemo-regioselective reaction
Hydrogenation
Acrolein
Crotonaldehyde
Prenal
Pt(1 1 1)
Heterogeneous catalysis
Density functional theory

ABSTRACT

On the basis of density functional theory calculations and an original use of a generalized Brönsted–Evans–Polanyi relationship, the key question of the change of selectivity has been solved for hydrogenation of three unsaturated aldehydes (acrolein, crotonaldehyde and prenal) on a Pt(1 1 1) surface. This study supports the idea that the selectivity in favor of the unsaturated alcohol (UOL) is controlled by adsorption thermodynamics of this partially hydrogenated product while the selectivity in favor of the other compound in competition (saturated aldehyde, SAL) obeys a more subtle kinetic control. The present work demonstrates the efficiency and the potentiality of the exposed correlation.

1. Introduction

Nowadays selectivity is an important aspect in chemistry and in heterogeneous catalysis in particular, for numerous industrial processes related to fine chemistry, pharmacology and environment [1,2]. The final goal is the obtainment of green chemistry for which the chemical wastes are either minimized or tolerable, i.e. all the byproducts of the considered reaction are desired and used.

Among the interesting reactions in heterogeneous catalysis, the selective hydrogenation of α,β-unsaturated aldehydes (UAL) on metallic catalysts has received much attention during the last thirty years. Several studies have demonstrated the potential applications for the synthesis of fine chemicals in perfume chemistry and pharmacology [3,4]. There are several factors which can affect the activity and the selectivity of the usual catalysts. These are the nature of the metal (Pt, Pd, Au, Ru, etc.) and of the support selection (SiO_2, Al_2O_3, etc.), metal precursor, catalyst preparation and activation methods, selection of reaction conditions (gas or liquid phase systems) [5–16]. The actual industrial reactant is citral [17–19]. However, due to the complexity of this molecule, several model compounds have been considered for systematic studies (cinnamaldehyde, prenal, crotonaldehyde, acrolein, etc.) [4,5,20]. Among the most active and selective catalysts, platinum has been retained in the majority of the published works [6–8,21,22]. In the considered experimental conditions [6,21] (978 mbar of H_2 and 33 mbar of UAL at 353 K), the authors have shown that the hydrogenation of the unsaturated aldehyde (cf. Fig. 1) yields three different products in competition; two alcohols (UOL and SOL) and one saturated aldehyde (SAL). ENOL is a partial hydrogenation byproduct which transforms itself during the reaction. The desired product is essentially UOL for fragrance chemistry and pharmaceuticals. However, the observed selectivities depend on the chemical nature of the model compound. In fact, for the hydrogenation of acrolein, the major product is SAL (92.6% see Table 1). Only a small fraction of UOL is produced (1.6%). Nonetheless, when terminal hydrogen atoms at the C=C bond of acrolein are substituted by one or two methyl groups (forming crotonaldehyde or prenal, respectively), the selectivity progressively changes in favor of the corresponding desired compound UOL (13.0% and 20.5%, respectively) but also in favor of the saturated alcohol SOL (33.6% and 55.0%, respectively). In other conditions and in particular for a lower conversion rate of

* Corresponding author. Fax: +33 4 72 72 88 60.
E-mail addresses: slimane.laref@ens-lyon.fr (S. Laref), francoise.delbecq@ens-lyon.fr (F. Delbecq), david.loffreda@ens-lyon.fr (D. Loffreda).
URL: http://perso.ens-lyon.fr/david.loffreda (D. Loffreda).

0021-9517/$ - see front matter © 2009 Elsevier Inc. All rights reserved.
doi:10.1016/j.jcat.2009.04.010

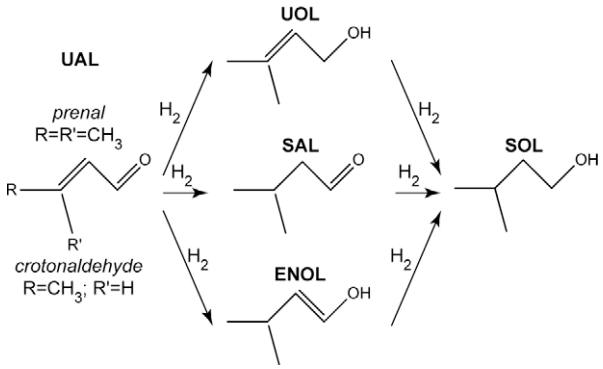

Fig. 1. Scheme exposing the possible products yielded during the selective hydrogenation of the unsaturated aldehydes (UAL, crotonaldehyde and prenal) on Pt catalyst. From a partial hydrogenation of one of the double bonds, two alcohols are obtained (unsaturated alcohol UOL and ENOL) and one saturated aldehyde SAL. The complete hydrogenation produces one saturated alcohol SOL.

Table 1
Experimental selectivities (%) observed for the hydrogenation of simple unsaturated aldehydes on Pt/Aerosil catalyst with partial pressures of 978 mbar of H_2 and 33 mbar of UAL at 353 K.

Pt catalysts		Selectivities %		
At low conversion [6]		SAL	UOL	SOL
Acrolein	R=R′=H	92.6	1.6	1.8
Crotonaldehyde	R=H; R′=CH_3	50.0	13.0	33.6
Prenal	R=R′=CH_3	17.0	20.5	55.0
At 20% conversion [21]				
Prenal		5.0	62.0	30.0

20%, the measured selectivity to UOL is even larger (62.0% for prenal hydrogenation). The fundamental explanation of such a change has stayed obscure during the last years. The electron-donor inductive effect has been evoked obviously without clearly solving the questions of the selectivity change. In particular, experimental observations are limited for explaining the selectivity changes observed for these aldehydes. In order to tackle such a problem, a better comprehension of the reaction mechanism and kinetics is required.

Among the possible approaches, theoretical investigations have been proposed to rationalize the adsorption and reactivity properties of the monometallic and bimetallic catalysts towards such a chemo-regioselective reaction [20,23–35]. After a first model using Extended Hückel calculations [23], Delbecq and Sautet have published a density functional theory study of the adsorption properties of acrolein, crotonaldehyde and prenal on the Pt(1 1 1) surface [20]. The authors have shown that various complex flat and vertical adsorption structures are possible for these aldehyde molecules. These preliminary results have been exhaustively confirmed by a reinvestigation of these catalytic systems by means of temperature programme desorption (TPD), high resolution electron energy loss spectroscopy (HREELS) measurements and density functional theory (DFT) simulations of the adsorbate vibrations and their corresponding vibrational spectra [24,29,30]. More recently, the hydrogenation pathways of acrolein on Pt(1 1 1) have been completely calculated using DFT and the Climbing-Image Nudged Elastic Band (CI-NEB) method [26–28]. The authors have shown that in contrast with the Rylander's empirical rule [36,37], the hydrogen attack at the C=O bond is always more favorable than the one at the C=C moiety [27]. They have also shown that the selectivity to SAL in the case of acrolein is essentially controlled by a compromise between desorption barriers that clearly favor the production of SAL and surface hydrogenation barriers that are in favor of the hydrogenation of C=O leading to UOL [26]. The final key result concerns the elaboration of a new family of correlations for acrolein on Pt(1 1 1) which propose a generalization of the more classical Brönsted–Evans–Polanyi (BEP) relationships [38,39]. The authors have demonstrated that hydrogenation activation energy barriers can be easily obtained by these relationships as soon as the coadsorption energy of the hydrogenation precursor state is calculated with standard DFT [28].

In this work, we propose an innovative approach for solving the questions of the selectivity changes between the hydrogenation of acrolein (reference case published before) and that of crotonaldehyde and prenal. In fact, we will calculate rapidly and accurately all the activation barriers for these latter molecules without exploring the hydrogenation pathways with the Nudged-Elastic Band methodology. To do so, we will intensively use and apply the generalized BEP relationship demonstrated previously for acrolein on Pt(1 1 1) [28] to the other molecules (crotonaldehyde and prenal) on the same surface. Only on the basis of the DFT calculations of the initial hydrogenation states, an explanation of the selectivity changes will be drawn and the electronic effect of the methyl substitution will be clarified from reaction thermodynamics and kinetics.

2. Methodology

The present study is based on density functional theory calculations which have been performed with VASP code [40,41] on periodic metallic slabs. All the results of the total electronic energy calculations exposed in the following have been performed at the generalized gradient approximation (GGA) with the Perdew Wang 91 exchange-correlation functional [42] and the projector-augmented-wave method (PAW) [43]. For the expansion of the plane-wave basis set, a converged cutoff has been set to 400 eV. The coverage chosen here on the Pt(1 1 1) surface (1/9 ML) is associated with a (3×3) supercell throughout the study. The Brillouin zone integration has been performed on a $(3 \times 3 \times 1)$ Monkhorst-Pack *k*-point mesh. The surface is modeled by a periodic slab composed of four metal layers and a vacuum of five equivalent metal layers (vacuum = 11.5 Å). Adsorption occurs only on one side of the slab. During all the geometry optimizations, the degrees of freedom of the adsorbate and the two uppermost metal layers have been relaxed while the two lowest metallic planes have been frozen in a bulk-like optimal geometry (2.82 Å).

3. Density functional theory calculations

In the classical Brönsted–Evans–Polanyi relation [38,39], the activation energy barrier is correlated with the reaction energy. Such a correlation has already been reported for the reactivity of small molecules on transition metal surfaces [44–50]. Recently, a density functional theory study of acrolein hydrogenation pathways on Pt(1 1 1) has evidenced that the adsorption energy of initial hydrogenation state is linearly correlated with the adsorption energy of transition state [28] (see the Supplementary materials for details). These initial states correspond systematically to coadsorption structures of hydrogen with crotonaldehyde or prenal reactant or any associated partially hydrogenated surface species (coadsorption energy, E^{IS}_{coads}). In order to solve the questions of the selectivity, the four different linear correlations are used as follows for each possible attack site (O1, C2, C3, C4) of the double bonds:

$$E^{TS}_{coads} = A \times E^{IS}_{coads} + B \quad (1)$$

$$E^{corr}_{act} = (A - 1) \times E^{IS}_{coads} + B \quad (2)$$

The used parameters for calculating the activation energy E_{act}^{corr} are recalled in Table 2. These linear relations are directly connected with the elementary steps of the complete hydrogenation mechanism of the unsaturated aldehydes on Pt(1 1 1).

According to the complete hydrogenation scheme, 32 different hydrogenation initial states have to be considered in the reaction mechanism in order to describe each of the elementary hydrogenation step:

$$(RH_{n-1} + H)_{coads} \rightarrow RH_n + Pt \quad (3)$$

In the model, the coadsorption energy of the initial or the transition state is calculated according to the following equation:

$$RH_{n-1,gas} + 1/2H_{2,gas} + Pt \rightarrow (RH_{n-1} + H)_{coads} \quad (4)$$

where the reactant $RH_{n-1,gas}$ can be a closed shell molecule in the gas phase or a radical species. The complete set of the optimized gas phase radicals is exposed in detail in the Supplementary materials (energetics, spin properties and geometries).

The originality of our approach is that the computational effort has been only focused on the geometry optimizations of the initial states associated with the 32 elementary acts evoked hereabove. These coadsorption structures are exposed in Figs. 2 and 3 for crotonaldehyde, and in Figs. 4 and 5 for prenal.

The corresponding coadsorption energies are reported in Table 3. The initial guesses of these structures are those previously found for acrolein hydrogenation. In these structures the hydrogen atom is mainly located in a threefold hollow site, and less commonly in a bridge or a top position. Usually, when the hydrogen attacks the oxygen atom of the C=O bond, it sits in a top position, whereas when the hydrogenation occurs at the C=C bond, the hydrogen atom is located in a threefold hollow site. The adsorption geometry of the reactant directly depends on the elementary step and on the hydrogenation degree of the intermediate hydrogenated species. For both crotonaldehyde and prenal hydrogenations, the molecule sits in a $\eta_2\mu_2$-trans or a $\eta_4\mu_4$-trans structure for the first hydrogenation step $+i$ ($i = 1,\ldots,4$). These coadsorption structures present a

Table 2
Parameters (A without units and B in eV) of the linear relations obtained for acrolein hydrogenation on Pt(1 1 1) between the coadsorption energy of the transition state TS and the one of the initial state IS (coadsorbed reactants).

$E_{coads}^{TS} = A \times E_{coads}^{IS} + B$	A	B	R^2
Hydrogenation at O1	1.0308	0.2785	0.9951
Hydrogenation at C2	0.8690	0.3391	0.9948
Hydrogenation at C3	1.0353	0.9034	0.9980
Hydrogenation at C4	1.0472	0.9149	0.9992

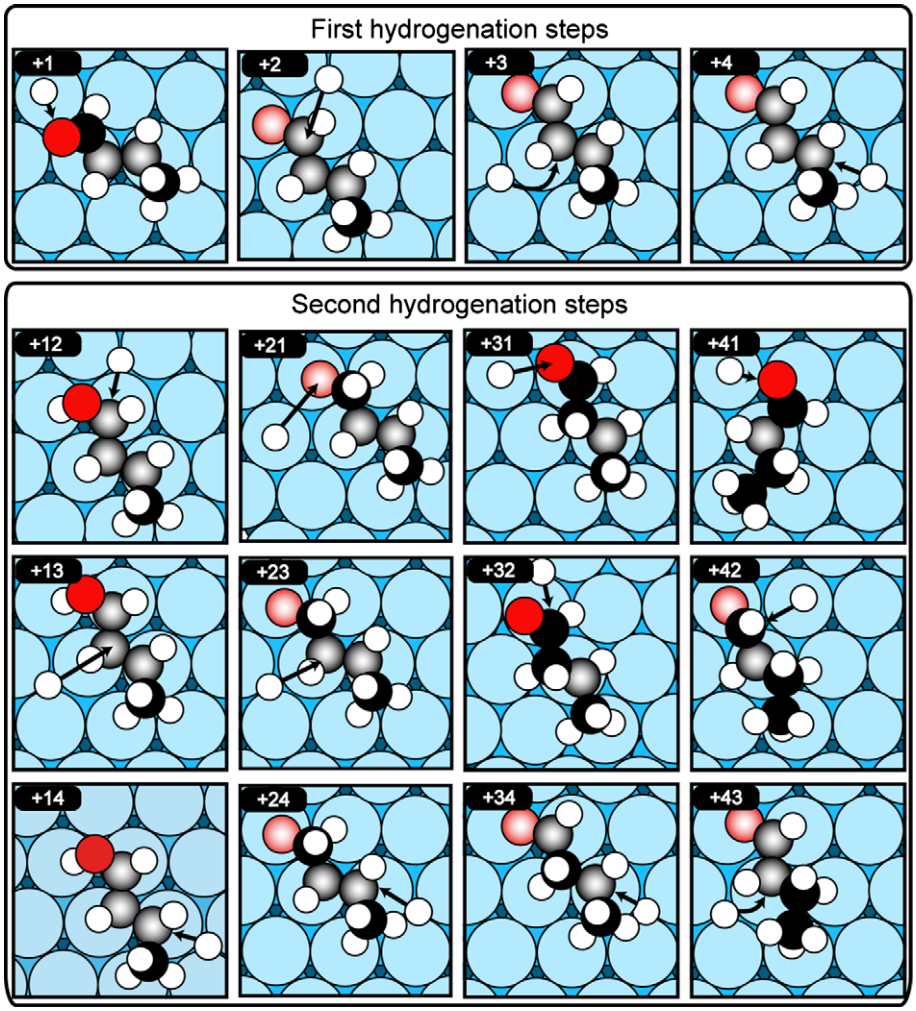

Fig. 2. Top views of the precursor states of each elementary step of the first ($+i$ addition) and second ($+ij$ addition) hydrogenations of crotonaldehyde on Pt(1 1 1). The black arrows define the hydrogen attack on oxygen atom O1 and on carbon atoms C2, C3 and C4. The shaded red (O1), and black (C2, C3, C4) balls indicate the atoms effectively bonded to the Pt surface. The corresponding coadsorption energies are listed in Table 3. (For interpretation of the references to colour in this figure legend, the reader is referred to the web version of this article.)

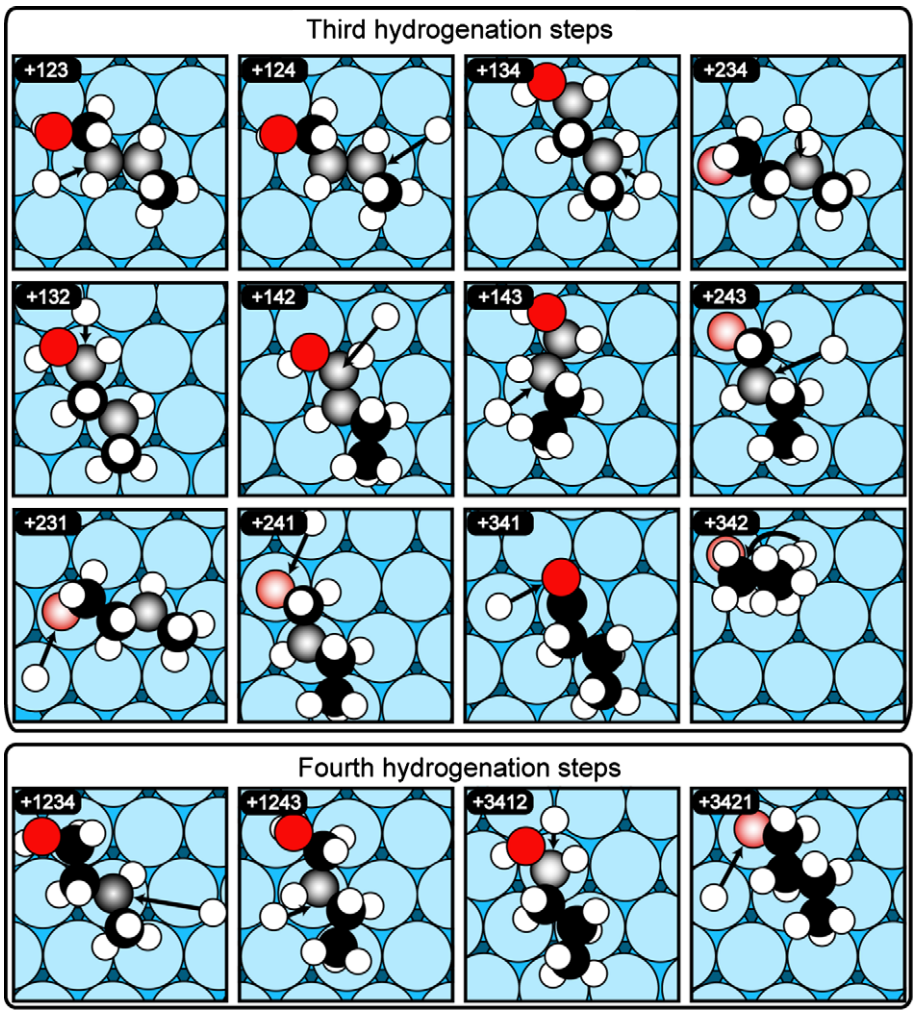

Fig. 3. Top views of the precursor states of each elementary step of the third (+*ijk* addition) and fourth (+*ijkl* addition) hydrogenations of crotonaldehyde on Pt(1 1 1). The black arrows define the hydrogen attack on oxygen atom O1 and on carbon atoms C2, C3 and C4. The shaded red (O1), and black (C2, C3, C4) balls indicate the atoms effectively bonded to the Pt surface. The corresponding coadsorption energies are listed in Table 3. (For interpretation of the references to colour in this figure legend, the reader is referred to the web version of this article.)

competitive stability (from −1.18 to −1.05 eV for crotonaldehyde and from −1.01 to −0.88 eV for prenal).

For the second hydrogenation routes +*ij*, the picture is more complex. Usually, the monohydrogenated species mh_i are typically chemisorbed in a $\eta_3\mu_3$-trans structure. However, a few exceptions exist when the attack occurs at the CHO moiety. For these cases, the monohydrogenated species can be adsorbed in $\eta_1\mu_1$-trans or $\eta_2\mu_2$-trans structure (see +31, +32, +41 and +42 in Figs. 2 and 4). Since the gas phase references have changed, the relative stability can be compared essentially for a fixed value of *i* in a series of +*ij*. As before, a similar stability is obtained for the coadsorption structures containing mh_1 species. A small decrease in the stability is observed for the prenal case, as before. The same remark can be done for the structures presenting mh_2, mh_3 and mh_4 surface intermediates.

Regarding the third hydrogenation steps +*ijk*, the adsorption geometry of the dih_{ij} species in the precursor states may change also significantly from an $\eta_2\mu_2$-trans position most of the time, to an $\eta_1\mu_1$-trans structure for +342 and even a pseudo-agostic form bonded through the hydrogen atom of the CHO group for +341. Among the precursor states, some of them are associated with the coadsorption of partial hydrogenation products such as UOL (dih_{12}), SAL (dih_{34}) and ENOL (dih_{14}). These products essentially adsorb in a $\eta_2\mu_2$-trans structure. The corresponding adsorption energies are different since these three compounds exhibit a different stability in the gas phase. The coadsorption structures with UOL are more strongly bonded to the surface (from −1.28 to −1.24 eV for crotonaldehyde and from −1.15 to −1.12 eV for prenal) than the ones with SAL (from −0.69 to −0.67 eV for crotonaldehyde and from −0.72 to −0.74 eV for prenal). Moreover, the precursor states with UOL are destabilized from crotonaldehyde to prenal, while they are slightly stabilized for the ones with SAL. This will have a significant impact on the selectivity, as it will be discussed in the next section. For the coadsorption structures with the other dihydrogenated species (dih_{13},dih_{23} and dih_{24}), the coadsorption energy are much stronger since the gas phase references correspond to high energy diradical species as it can be seen in the Supplementary materials.

The complete hydrogenation of the unsaturated aldehydes then occurs with the fourth hydrogenation routes +*ijkl*. In these last four cases, the precursor states involve trihydrogenated surface species th_{ijk} adsorbed in an $\eta_1\mu_1$-trans form.

Once all the precursor states have been optimized, the linear relations have been applied to estimate the coadsorption energy of the transition state and the activation energy for each case from the calculated coadsorption energy of the initial state (see Eqs. (1)

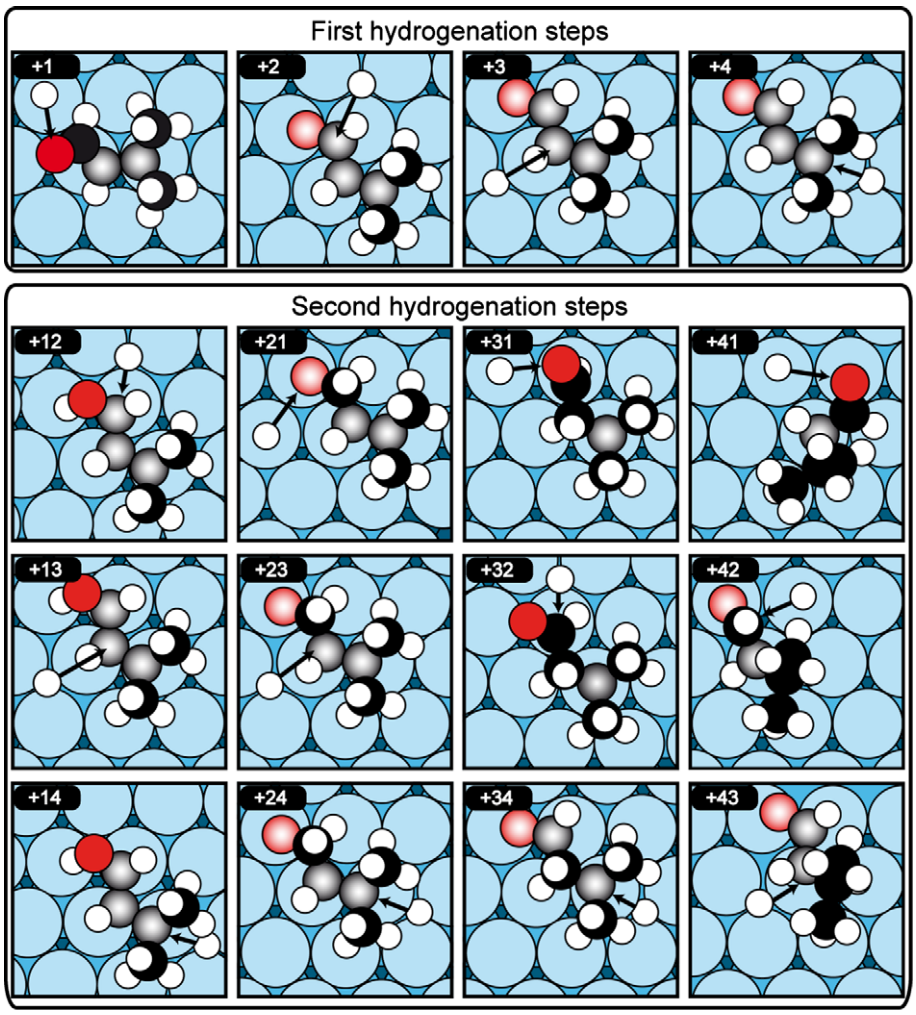

Fig. 4. Top views of the precursor states of each elementary step of the first (+*i* addition) and second (+*ij* addition) hydrogenations of prenal on Pt(1 1 1). The black arrows define the hydrogen attack on oxygen atom O1 and on carbon atoms C2, C3 and C4. The shaded red (O1), and black (C2, C3, C4) balls indicate the atoms effectively bonded to the Pt surface. The corresponding coadsorption energies are listed in Table 3. (For interpretation of the references to colour in this figure legend, the reader is referred to the web version of this article.)

and (2) and Table 2). In order to compare the activation energies coming from the application of the relations E_{act}^{corr} for crotonaldehyde and prenal with the ones effectively calculated from the Nudged-Elastic Band method for acrolein E_{act}^{NEB}, all these results have been reported in Table 3. In agreement with the key findings exposed previously for acrolein [27,28], the ordering of the activation barriers for crotonaldehyde and prenal hydrogenation on Pt(1 1 1) is ruled as follows: The attack at the C=O bond is always more favorable than the one at the C=C bond. For acrolein, the attack at the oxygen atom of the C=O bond ranges from 0.02 to 0.43 eV. For crotonaldehyde and prenal, the same elementary steps are associated with barriers ranging from 0.17 to 0.26 eV, and from 0.18 to 0.26 eV, respectively. Regarding the hydrogenation at the carbon atom of the C=O bond, the activation energy is higher for acrolein (from 0.41 to 0.88 eV). Similar values are obtained for crotonaldehyde (from 0.43 to 0.87 eV) and for prenal (from 0.26 to 0.85 eV). Finally, the largest barriers occur almost systematically for the attacks at the C=C bond. A last remark concerns the nature of the hydrogenation elementary mechanism. In absolute agreement with the case of acrolein on Pt(1 1 1), the hydrogenation at the oxygen of the C=O bond follows a new type of mechanism for crotonaldehyde and prenal on the same surface. This mechanism is intermediate between Langmuir–Hinshelwood and Rideal–Eley since the CHO moiety is decoordinated from the Pt surface when the hydrogen atom attacks the double bond. In contrast, the attacks at the C=C bond obey the usual Langmuir–Hinshelwood mechanism for both molecules on Pt(1 1 1) (crotonaldehyde and prenal), as for acrolein.

4. Discussion

Before discussing in more detail the calculated changes of the activation energy for the hydrogenation of the three reactants on Pt(1 1 1), a few words should be devoted to the comparison of the key hydrogenation products UOL and SAL (cf. Fig. 6 for the adsorption structures and energies). In fact, the stronger adsorption of the UOL product is more affected by the methyl substitution (from −1.08 eV for the UOL of acrolein in a diσ(CC) structure, to −0.89 and −0.80 eV for the UOL of crotonaldehyde and prenal, respectively), whereas the weaker interaction between SAL and Pt is less modified (from −0.23 eV for the SAL of acrolein in a diσ(CO) form to −0.22 and −0.20 eV for the SAL of crotonaldehyde and prenal, respectively).

The determination of all the activation energy barriers for the complete hydrogenation scheme of the three unsaturated

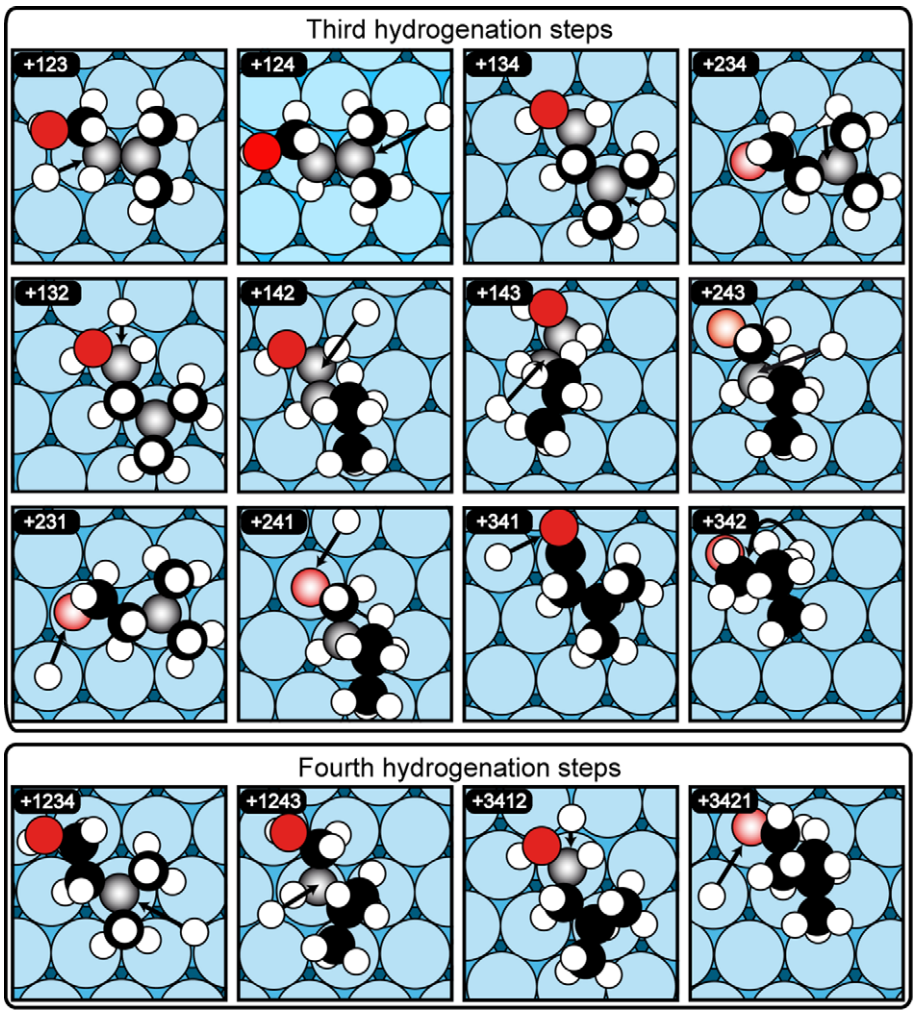

Fig. 5. Top views of the precursor states of each elementary step of the third (+*ijk* addition) and fourth (+*ijkl* addition) hydrogenations of prenal on Pt(1 1 1). The black arrows define the hydrogen attack on oxygen atom O1 and on carbon atoms C2, C3 and C4. The shaded red (O1), and black (C2, C3, C4) balls indicate the atoms effectively bonded to the Pt surface. The corresponding coadsorption energies are listed in Table 3. (For interpretation of the references to colour in this figure legend, the reader is referred to the web version of this article.)

aldehydes is the last key ingredient for answering the question of selectivity. Therefore the variations of the activation energy barriers between crotonaldehyde (or prenal) and acrolein are addressed in Figs. 7 and 8 for the first and second hydrogenation routes, and the third and the fourth hydrogenation steps, respectively. The corresponding variations are also reported in Table 3. Now that the picture of kinetics is completed, we examine first the case of crotonaldehyde. In Fig. 7, the activation barrier variations have been exposed for the first and the second hydrogenation steps. A significant increase of the barrier (>0.1 eV) from acrolein to crotonaldehyde (or prenal) appears with a red arrow and a red value of the energy, whereas a substantial decrease of the barrier (<−0.1 eV) is mentioned with a green arrow and a green value. Intermediate cases cannot be really considered as a significant change due to the accuracy of our DFT calculations and the accuracy of the correlation model (50 meV). They appear with blue arrows and values. A preliminary remark is related to the majority of the barrier variations ΔE which are effectively weak (blue values) and intermediate in the range $-0.1 < \Delta E < 0.1$ eV. In particular, the barriers for transforming crotonaldehyde into UOL and SAL are almost non-affected by the methyl substitution on acrolein. A significant change of the barriers is visible for the competitive second hydrogenation routes transforming mh_3 into dih_{23} (a decrease in the activation energy of −0.12 eV) and transforming mh_4 into ENOL or dih_{24} (increases of the barriers of +0.20 and +0.17 eV, respectively). These results are in favor of an increase of the formation of dih_{23} and a weakening of the production of ENOL and dih_{24} for crotonaldehyde by comparison with the case of acrolein. When the analysis is carried on with the third and the fourth hydrogenation elementary steps (see Fig. 8), a clear discrepancy appears now between the key products in competition UOL and SAL. Indeed, the transformation of UOL into SOL either shows non-variation compared to acrolein (third steps) or exhibits a significant increase of the barriers (fourth steps). In contrast, the transformation of SAL into SOL shows an effective decrease in the activation energies for the third (−0.17 eV) and the fourth hydrogenation steps (−0.13 eV) through the th_{134} route. Hence, in the complete hydrogenation scheme, the routes yielding UOL and SAL are unperturbed from acrolein to crotonaldehyde, whereas the further transformation of UOL into SOL is slowed down and the further transformation of SAL into SOL is sped up. This picture is non-modified by the last possibility coming from the transformation of dih_{23} into SOL (cf. Fig. 8).

As an intermediate conclusion for crotonaldehyde, the present study demonstrates the existence of two different controls for the change of selectivity. The formation of UOL at the Pt(1 1 1) surface is not affected by the methyl substitution from the kinetic point of view. However, this product desorbs more easily from the surface when the C=C bond is substituted. The consequence

Table 3
Application of the linear relations obtained for acrolein on Pt(1 1 1) for the cases of the hydrogenation of crotonaldehyde and prenal on the same surface. All the energies are expressed in eV. For each elementary step, the DFT barrier for acrolein is recalled [27,28]. The coadsorption energy of the precursor states E^{IS}_{coads} (crotonaldehyde and prenal) is given with the corresponding activation energy E^{corr}_{act} resulting from the application of the formulae derived in Eqs. (1) and (2) and are also given in Table 2. The activation barrier deviations ΔE between acrolein and crotonaldehyde, or acrolein and prenal are also listed and reported in Figs. 7 and 8.

eV	Acrolein	Crotonaldehyde			Prenal		
	E^{NEB}_{act}	E^{IS}_{coads}	E^{corr}_{act}	ΔE	E^{IS}_{coads}	E^{corr}_{act}	ΔE
TS_1	0.19	−1.05	0.25	0.06	−0.88	0.25	0.06
TS_2	0.51	−1.13	0.49	−0.02	−0.96	0.46	−0.05
TS_3	0.84	−1.18	0.83	−0.01	−1.01	0.84	−0.01
TS_4	0.83	−1.15	0.85	0.02	−0.98	0.86	0.02
TS_{12}	0.69	−2.34	0.65	−0.04	−2.11	0.61	−0.07
TS_{13}	0.82	−2.44	0.81	−0.01	−2.20	0.82	−0.01
TS_{14}	0.83	−2.34	0.80	−0.03	−2.10	0.81	−0.02
TS_{21}	0.20	−2.63	0.20	−0.00	−2.40	0.20	0.00
TS_{23}	0.84	−2.62	0.81	−0.03	−2.40	0.81	−0.03
TS_{24}	0.83	−2.64	0.78	−0.05	−2.43	0.79	−0.04
TS_{31}	0.18	−2.02	0.21	0.03	−1.86	0.22	0.03
TS_{32}	0.73	−2.03	0.61	−0.12	−1.78	0.57	−0.16
TS_{34}	0.85	−2.01	0.81	−0.04	−1.84	0.82	−0.03
TS_{41}	0.02	−1.71	0.22	0.20	−1.75	0.22	0.20
TS_{42}	0.41	−1.83	0.58	0.17	−1.76	0.57	0.16
TS_{43}	0.84	−1.85	0.82	−0.02	−1.84	0.82	−0.02
TS_{123}	0.83	−1.28	0.83	−0.00	−1.12	0.83	0.00
TS_{124}	0.81	−1.24	0.84	0.03	−1.15	0.85	0.03
TS_{132}	0.88	−4.03	0.87	−0.01	−3.87	0.85	−0.03
TS_{134}	0.72	−4.04	0.72	−0.00	−3.88	0.73	0.00
TS_{142}	0.41	−0.84	0.45	0.04	−0.86	0.45	0.04
TS_{143}	0.92	−1.27	0.83	−0.09	−1.25	0.83	−0.08
TS_{231}	0.18	−3.32	0.17	−0.01	−1.10	0.24	0.06
TS_{234}	0.66	−3.22	0.75	0.09	−1.02	0.85	0.19
TS_{241}	0.25	−3.22	0.18	−0.07	−3.01	0.18	−0.06
TS_{243}	0.79	−3.24	0.80	0.01	−3.03	0.80	0.02
TS_{341}	0.43	−0.67	0.26	−0.17	−0.74	0.26	−0.17
TS_{342}	0.51	−0.69	0.43	−0.08	−0.72	0.26	−0.25
TS_{1234}	0.70	−2.21	0.80	0.10	−1.98	0.81	0.11
TS_{1243}	0.73	−2.01	0.82	0.09	−1.94	0.82	0.10
TS_{3412}	0.77	−2.22	0.63	−0.14	−2.29	0.64	−0.13
TS_{3421}	0.21	−2.00	0.22	0.01	−2.50	0.20	0.00

should be an increase in the selectivity to UOL from acrolein to crotonaldehyde. Our result agrees with the experimental observations (cf. Table 1). This supports the idea of a thermodynamic control for the corresponding selectivity change. For the formation of SAL or its desorption, no significant change appears from the kinetic or the thermodynamic point of view. Nevertheless, the transformation of SAL into SOL is effectively facilitated from acrolein to crotonaldehyde. This should result in an effective decrease in the selectivity to SAL and an increase in the one to SOL. Our assumptions based on DFT results are fully compatible with experiments. Hence, the selectivity to SAL and SOL is controlled by kinetics.

According to experiments, the change of the selectivity in favor of SAL and SOL is even clearer for prenal (cf. Table 1). By examining our schemes for this last molecule, the argumentation is still valid for the thermodynamic control of UOL since the activation barrier changes are absolutely comparable with the ones of crotonaldehyde. Hence the weakened adsorption strength of this product should be responsible for the increase of selectivity. For the kinetic control of the selectivity to SAL and SOL, the trend is even more clear-cut for prenal, since the transformation of SAL into SOL via the th_{234} route is also sped up (−0.25 eV). Hence, our assumptions of a thermodynamic control for the selectivity to UOL and a kinetic one for the selectivity to SAL and SOL are supported by the investigation of the reactivity of both crotonaldehyde and prenal molecules.

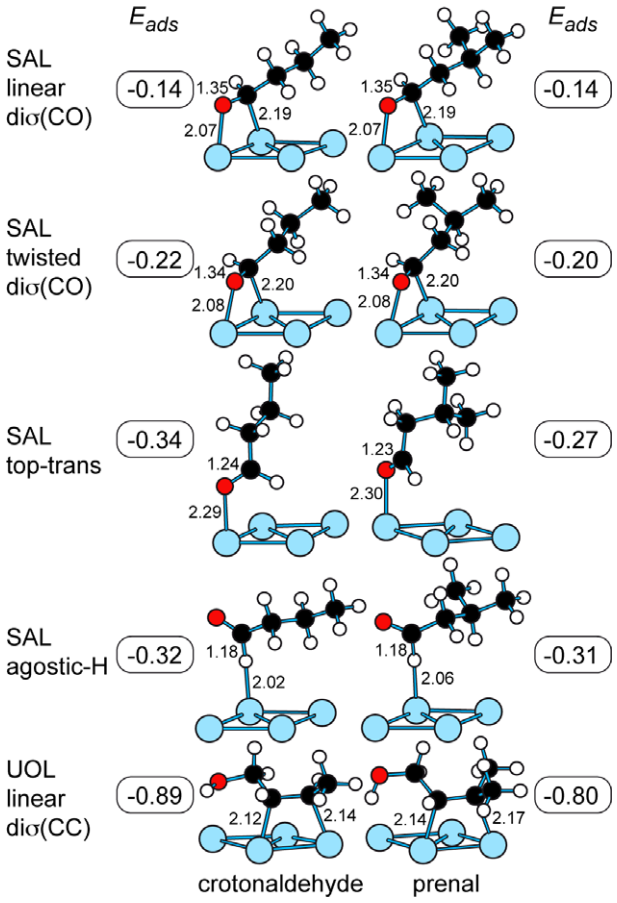

Fig. 6. Optimized adsorption structures (key distances in Å) and adsorption energies E_{ads} (eV) of SAL and UOL products corresponding to crotonaldehyde and prenal hydrogenation, respectively.

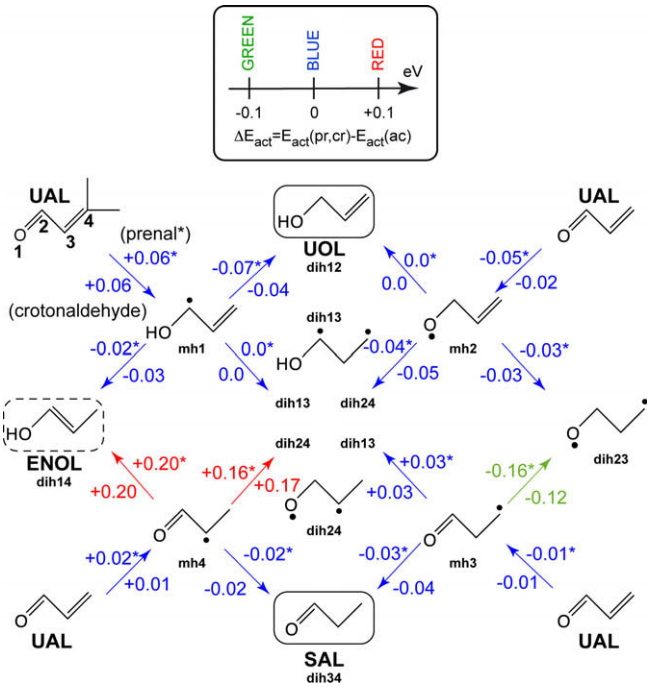

Fig. 7. Scheme of the elementary steps of the first and second hydrogenations for crotonaldehyde and prenal on Pt(1 1 1). For each molecule, the activation energy deviations ΔE (eV) are given by comparison with the reference case (acrolein on Pt(1 1 1)). The barriers for prenal appear with a star and are given above the arrows. The corresponding values are also listed in Table 3.

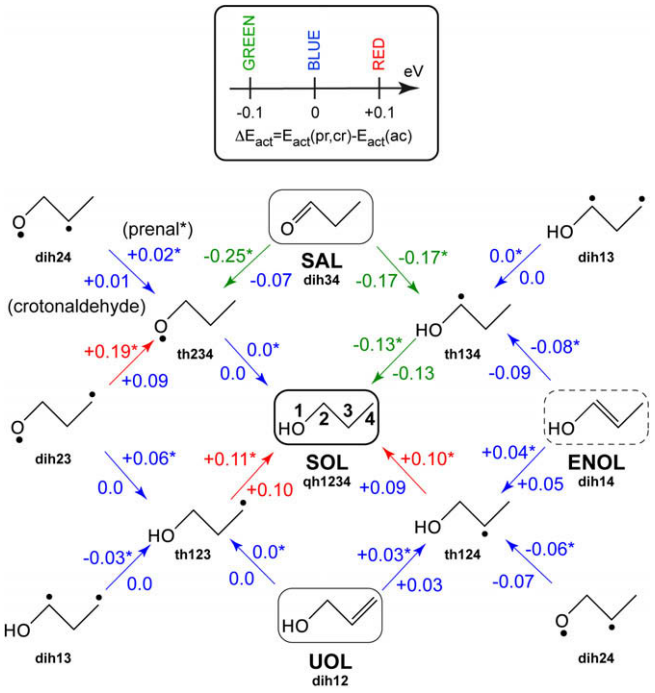

Fig. 8. Scheme of the elementary steps of the third and fourth hydrogenations for crotonaldehyde and prenal on Pt(1 1 1). For each molecule, the activation energy deviations ΔE (eV) are given by comparison with the reference case (acrolein on Pt(1 1 1)). The barriers for prenal appear with a star and are given above the arrows. The corresponding values are also listed in Table 3.

5. Conclusion

In this study, the question of the change of selectivity observed experimentally for the hydrogenation of simple unsaturated aldehydes on Pt catalyst has been addressed by a combination of density functional theory calculations and a generalized Brönsted–Evans–Polanyi correlation. According to the estimation of all the activation energy barriers for the hydrogenation routes and to the calculations of the desorption barriers for the products in competition, the methyl substitution of acrolein progressively leading to crotonaldehyde and prenal has two major impacts on the selectivity of the Pt(1 1 1) surface: a thermodynamic control for the UOL compound and a kinetic control for the SAL and the SOL products. The enhanced selectivity to UOL observed from acrolein to crotonaldehyde and prenal is controlled by the stability of the adsorbed product. The weakening of the adsorption strength due to the methyl substitution favors the selectivity to UOL. The increased selectivity to SOL is conversely controlled by a lowering of the hydrogenation barriers transforming SAL into SOL which finally favors the formation of SOL in the detriment of the one of SAL.

The remarkable agreement between our DFT analysis and the experimental conclusions hence allows an explanation of the measurements. Moreover, it demonstrates the efficiency of the use of the generalized BEP correlations for the hydrogenation of simple unsaturated aldehydes on a metal catalyst. In fact, our study effectively shows that these relations are predictive and that they allow a fast and accurate estimation of the reaction barriers. In conclusion, our systematic theoretical approach of the reactivity in heterogeneous catalysis opens promising perspectives for the determination of the selectivity in future investigations.

Acknowledgments

The authors thank IDRIS at Orsay, CINES at Montpellier (Project 609) and PSMN at Lyon for CPU time and assistance. They acknowledge CNRS-DFG bilateral project and SIRE ANR contract for financial support.

Appendix A. Supplementary data

Supplementary data associated with this article can be found, in the online version, at doi:10.1016/j.jcat.2009.04.010.

References

[1] M. Bartok, K. Felföldi, Stereochemistry of Heterogeneous Metal Catalysis, Wiley, Chichester, 1985 (Chapter VII).
[2] R.L. Augustine, Heterogeneous Catalysis for the Synthetic Chemists, Marcel Dekker, New York, 1996.
[3] K. Bauer, D. Garbe, Common Fragrance and Flavor Materials, VCH, New York, 1985.
[4] P. Gallezot, D. Richard, Catal. Rev. Sci. Eng. 40 (1998) 81.
[5] P. Mäki-Arvela, J. Hájek, T. Salmi, D.Y. Murzin, Appl. Catal. A Gen. 292 (2005) 1.
[6] T.B.L.W. Marinelli, S. Nabuurs, V. Ponec, J. Catal. 151 (1995) 431.
[7] T.B.L.W. Marinelli, V. Ponec, J. Catal. 156 (1995) 51.
[8] V. Ponec, Appl. Catal. A Gen. 149 (1997) 27.
[9] A. Huidobro, A. Sepúlveda-Escribano, F. Rodríguez-Reinoso, J. Catal. 212 (2002) 94.
[10] F. Ammari, J. Lamotte, R. Touroude, J. Catal. 221 (2004) 32.
[11] B.C. Campo, S. Ivanova, C. Gigola, C. Petit, M.A. Volpe, Catal. Tod. 133–135 (2008) 661.
[12] B. Campo, C. Petit, M.A. Volpe, J. Catal. 254 (2008) 71.
[13] S. Schimpf, M. Lucas, C. Mohr, U. Rodemerck, A. Brückner, J. Radnik, H. Hofmeister, P. Claus, Catal. Tod. 72 (2002) 63.
[14] P. Claus, Top. Catal. 5 (1998) 51.
[15] C. Mohr, H. Hofmeister, J. Radnik, P. Claus, J. Am. Chem. Soc. 125 (2003) 1905.
[16] M. Bron, D. Teschner, A. Knop-Gericke, F.C. Jentoft, J. Kröhnert, J. Hohmeyer, C. Volckmar, B. Steinhauer, R. Schlögl, P. Claus, Phys. Chem. Chem. Phys. 9 (2007) 3559.
[17] U.K. Singh, M.A. Vannice, J. Catal. 191 (2000) 165.
[18] U.K. Singh, M.N. Sysak, M.A. Vannice, J. Catal. 191 (2000) 181.
[19] U.K. Singh, M.A. Vannice, J. Catal. 199 (2001) 73.
[20] F. Delbecq, P. Sautet, J. Catal. 211 (2002) 398.
[21] T. Birchem, C.-M. Pradier, Y. Berthier, G. Cordier, J. Catal. 146 (1994) 503.
[22] P. Beccat, J.-C. Bertolini, Y. Gauthier, J. Massardier, P. Ruiz, J. Catal. 126 (1990) 451.
[23] F. Delbecq, P. Sautet, J. Catal. 152 (1995) 217.
[24] D. Loffreda, Y. Jugnet, F. Delbecq, J.-C. Bertolini, P. Sautet, J. Phys. Chem. B 108 (2004) 9085.
[25] D. Loffreda, F. Delbecq, P. Sautet, Chem. Phys. Lett. 405 (2005) 434.
[26] D. Loffreda, F. Delbecq, F. Vigné, P. Sautet, Angew. Chem. Int. Ed. 44 (2005) 5279.
[27] D. Loffreda, F. Delbecq, F. Vigné, P. Sautet, J. Am. Chem. Soc. 128 (2006) 1316.
[28] D. Loffreda, F. Delbecq, F. Vigné, P. Sautet, J. Am. Chem. Soc. (2009), submitted for publication.
[29] J. Haubrich, D. Loffreda, F. Delbecq, Y. Jugnet, P. Sautet, A. Krupski, C. Becker, K. Wandelt, Chem. Phys. Lett. 433 (2006) 188.
[30] J. Haubrich, D. Loffreda, F. Delbecq, P. Sautet, Y. Jugnet, A. Krupski, C. Becker, K. Wandelt, J. Phys. Chem. C 112 (2008) 3701.
[31] R. Alcalá, J. Greeley, M. Mavrikakis, J.A. Dumesic, J. Chem. Phys. 116 (2002) 8973.
[32] K.H.L. Lim, Z.-X. Chen, K.M. Neyman, N. Rösch, Chem. Phys. Lett. 420 (2006) 60.
[33] L.E. Murillo, A.M. Goda, J.G. Chen, J. Am. Chem. Soc. 129 (2007) 7101.
[34] L.E. Murillo, J.G. Chen, Surf. Sci. 602 (2008) 919.
[35] L.E. Murillo, J.G. Chen, Surf. Sci. 602 (2008) 2412.
[36] P.N. Rylander, Catalytic Hydrogenation in Organic Syntheses, Academic Press, New York, 1979.
[37] P.N. Rylander, Hydrogenation Methods, Academic Press, London, 1985.
[38] J.N. Brönsted, Chem. Rev. 5 (1928) 231.
[39] M.G. Evans, M. Polanyi, Trans. Faraday Soc. 34 (1938) 11.
[40] G. Kresse, J. Hafner, Phys. Rev. B 47 (1993) 558.
[41] G. Kresse, J. Furthmüller, Phys. Rev. B 54 (1996) 11169.
[42] J.P. Perdew, Y. Wang, Phys. Rev. B 45 (1992) 13244.
[43] G. Kresse, D. Joubert, Phys. Rev. B 59 (1999) 1758.
[44] J.K. Nørskov, T. Bligaard, A. Logadottir, S. Bahn, L.B. Hansen, M. Bollinger, H. Bengaard, B. Hammer, Z. Sljivancanin, M. Mavrikakis, Y. Xu, S. Dahl, C.J.H. Jacobsen, J. Catal. 209 (2002) 275.
[45] T. Bligaard, J.K. Nørskov, S. Dahl, J. Matthiesen, C.H. Christensen, J. Sehested, J. Catal. 224 (2004) 206.
[46] A. Logadottir, T.H. Rod, J.K. Nørskov, B. Hammer, S. Dahl, C.J.H. Jacobsen, J. Catal. 197 (2001) 229.
[47] Z.-P. Liu, P. Hu, J. Chem. Phys. 114 (2001) 8244.
[48] V. Pallassana, M. Neurock, J. Catal. 191 (2000) 301.
[49] A. Michaelides, Z.-P. Liu, C.J. Zhang, A. Alavi, D.A. King, P. Hu, J. Am. Chem. Soc. 125 (2003) 3704.
[50] B. Hammer, Top. Catal. 37 (2006) 3.